TU Delft

Delft University of Technology

Photogeneration and Mobility of Charge Carriers in Atomically Thin Colloidal InSe Nanosheets Probed by Ultrafast Terahertz Spectroscopy

Lauth, Jannika; Kulkarni, Aditya; Spoor, Frank C M; Renaud, Nicolas; Grozema, Ferdinand C.; Houtepen, Arjan J.; Schins, Juleon M.; Kinge, Sachin; Siebbeles, Laurens D A

DOI
10.1021/acs.jpclett.6b01835

Publication date
2016

Document Version
Accepted author manuscript

Published in
The Journal of Physical Chemistry Letters

Citation (APA)
Lauth, J., Kulkarni, A., Spoor, F. C. M., Renaud, N., Grozema, F. C., Houtepen, A. J., Schins, J. M., Kinge, S., & Siebbeles, L. D. A. (2016). Photogeneration and Mobility of Charge Carriers in Atomically Thin Colloidal InSe Nanosheets Probed by Ultrafast Terahertz Spectroscopy. *The Journal of Physical Chemistry Letters*, *7*(20), 4191-4196. https://doi.org/10.1021/acs.jpclett.6b01835

Important note
To cite this publication, please use the final published version (if applicable).
Please check the document version above.

Copyright
Other than for strictly personal use, it is not permitted to download, forward or distribute the text or part of it, without the consent of the author(s) and/or copyright holder(s), unless the work is under an open content license such as Creative Commons.

Takedown policy
Please contact us and provide details if you believe this document breaches copyrights.
We will remove access to the work immediately and investigate your claim.

This work is downloaded from Delft University of Technology.
For technical reasons the number of authors shown on this cover page is limited to a maximum of 10.

This is an Accepted Author Manuscript of an article published by ACS in the Journal of Physical Chemistry Letters, available online: http://dx.doi.org/10.1021/acs.jpclett.6b01835

Photogeneration and Mobility of Charge Carriers in Atomically Thin Colloidal InSe Nanosheets Probed by Ultrafast Terahertz Spectroscopy

Jannika Lauth, [¥*] *Aditya Kulkarni,* [¥] *Frank C. M. Spoor,* [¥] *Nicolas Renaud,* [¥] *Ferdinand C. Grozema,* [¥] *Arjan J. Houtepen,* [¥] *Juleon M. Schins,* [¥] *Sachin Kinge,* [‡] *Laurens D. A. Siebbeles*[¥*]

[¥] Chemical Engineering Department, Delft University of Technology, Van der Maasweg 9, NL-2629 HZ Delft, The Netherlands

[‡] Toyota Motor Europe, Materials Research & Development, Hoge Wei 33, B-1930, Zaventem, Belgium

Abstract

The implementation of next generation ultrathin electronics by applying highly promising dimensionality-dependent physical properties of two-dimensional (2D) semiconductors is ever increasing. In this context, the van der Waals layered semiconductor InSe has proven its potential as photodetecting material with high charge carrier mobility. We have determined the photogeneration charge carrier quantum yield and mobility in atomically thin colloidal InSe nanosheets (inorganic layer thickness 0.8 – 1.7 nm, mono-/double-layers, ≤5 nm including ligands) by ultrafast transient terahertz (THz) spectroscopy. A near unity quantum yield of free charge carriers is determined for low photoexcitation density. The charge carrier quantum yield decreases at higher excitation density, due to recombination of electrons and holes, leading to the formation of neutral excitons. In the THz frequency domain we probe a charge mobility as high as 20 ± 2 cm^2/Vs. The THz mobility is similar to field-effect transistor mobilities extracted from unmodified exfoliated thin InSe devices. The current work provides the first results on charge carrier dynamics in ultrathin colloidal InSe nanosheets.

TOC Image

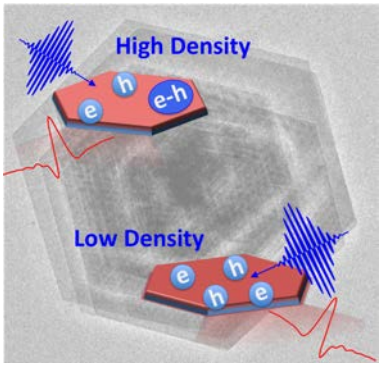

Two-dimensional (2D) semiconductors have gained steadily increasing interest in recent years due to physical properties, which are significantly different from their bulk counterparts. The tunability of the optical and electronic properties by variation of material thickness and composition offers promising prospects for application in optoelectronic devices[1-4] with high charge mobilities[5] and efficient charge carrier multiplication.[6]

InSe is a layered 2D van der Waals structure, which has been successfully applied as highly responsive (87 μs) photodetector[7] and in field-effect transistors (FETs) with high charge mobility (μ = 1000 cm^2/Vs).[5, 8] A single layer of InSe consists of 2 Se^{2-} anions and a $[In_2]^{4+}$ diatomic cation forming a weak internal In-In bond that leads to the formation of the common hexagonal Se-In-In-Se structure.[9-10] Multiple layers of InSe are usually exfoliated mechanically with Scotch tape from single crystals grown by the Bridgman method.[11-12] A technologically more relevant way to solution-processes ultrathin InSe has been recently presented by Lauth *et al*.[9] The colloidal method yields atomically thin InSe nanosheets (inorganic layer 0.8 – 1.7 nm, mono-/double-layer, total thickness ≤5 nm including ligands) that are separated from each other by organic ligands. Their optical absorption near 600 nm (2.1 eV) is significantly blue-shifted from the band gap of bulk InSe at 953 nm (1.3 eV[13]) (see Fig. 1 for optical absorption and TEM image). Ultrathin InSe nanosheets obtained by this method enable band gap tuning into higher energy regions that are scarcely reachable by exfoliated InSe layers.[14] InSe undergoes a direct-to-indirect band gap transition when reducing its layer thickness (see Fig. 2 for band structure), which causes a decrease of the photoluminescence (PL) efficiency.[9, 15] Interestingly, the PL efficiency of thin InSe layers could be enhanced recently by nanotexturing.[14]

Until now, no time-resolved spectroscopic methods have been applied to assess the charge carrier photogeneration, mobility and decay in ultrathin InSe. In the present work, we use time-

resolved terahertz (THz) conductivity measurements, which allow us to distinguish free electrons and holes from bound electron-hole pairs in the form of excitons. We probe the photogeneration charge carrier quantum yield and mobility in ultrathin colloidal InSe nanosheets and find a quantum yield near unity under low excitation density, while at higher density also excitons are formed. The THz mobility of free charge carriers in InSe nanosheets is as high as 20 ± 2 cm^2/Vs.

We synthesized ultrathin InSe nanosheets analogously to the method described in ref. 9 (see Supporting Information), except for exchanging the ligand octadecylamine by decylamine. InSe nanosheets with lateral sizes of 1-2 μm and the same original thickness of 0.8 – 1.7 nm (mono-/double-layers, see Fig. 1) are obtained. The optical absorption spectrum of a film of drop-casted InSe nanosheets shown in Fig. 1a exhibits an onset near 800 and lacks eminent features, similar to the ultrathin InSe nanosheets described previously (see Fig. S1 for absorption spectrum in solution with slight feature at ~600 nm).[9] Effects due to reflection or scattering from the samples are directly accounted for by performing absorption measurements inside an integrating sphere. The PL spectrum is broad with a maximum at 590 nm (see Fig. S1), originating from weak radiative recombination.[9] At short wavelengths the absorption spectrum in Fig. 1a levels off at 60 %, the remaining fraction of light is reflected.

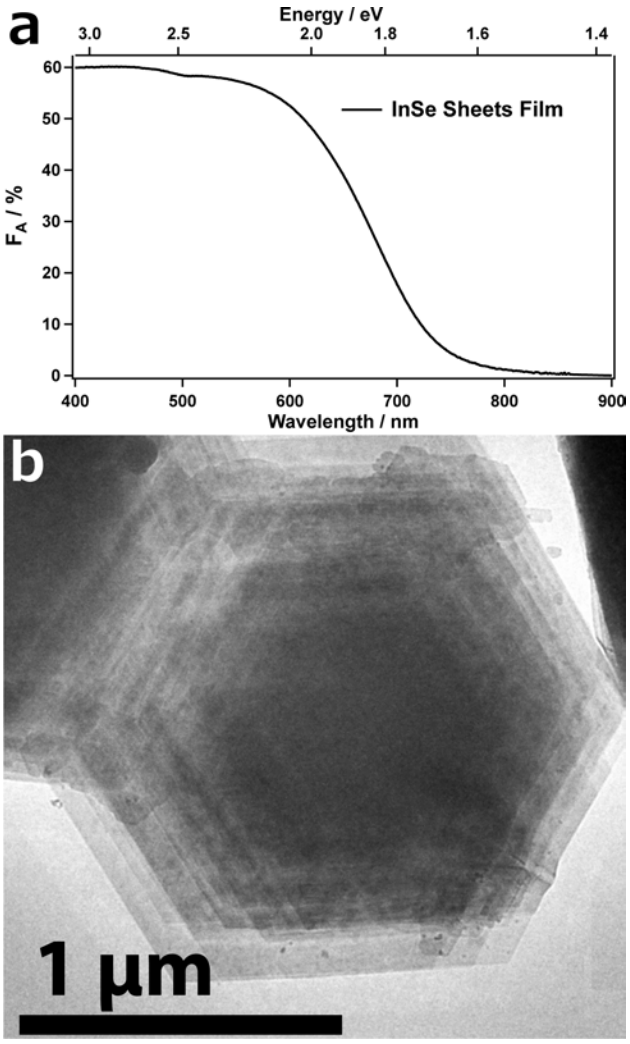

Fig. 1. a) Fraction of photons absorbed (F_A in %) by a drop-casted film of InSe nanosheets with the spectrum leveling off at 60 % for shorter wavelengths due to reflection of the remaining fraction of light. **b)** TEM image of a typical stack of InSe nanosheets with lateral sizes of 1 – 2 μm and a thickness of 0.8 - 1.7 nm.

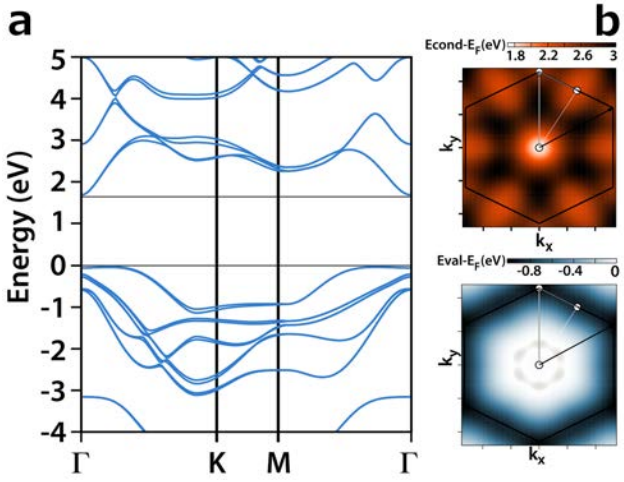

Fig. 2. a) Calculated band structure of a four-atomic InSe monolayer, with a slightly indirect band gap of 1.8 eV. The conduction band minimum is at the Γ point, while the valence band maximum lies between the Γ and the K point. **b)** Contour plots of the conduction and valence band in the first Brillouin zone. Note the flat character of the valence band.

The band structure of an InSe monolayer obtained by DFT calculations (see Experimental and Methods) is presented in Fig. 2. Fig. 2a shows the band dispersion along the Γ-K-M-Γ path in the Brillouin zone. The calculated band gap of 1.8 eV is indirect with the valence band maximum between the Γ and the K point, while the conduction band minimum is at Γ (also valid for an InSe bilayer not shown here).[16-17] The 2D dispersion of the conduction and valence bands in the first Brillouin zone is shown as contour plots in Fig. 2b. It can be seen that the valence band is very flat leading to a hole effective mass at the top of the valence band of at least one order of magnitude higher than the electron effective mass (see Experimental and Methods). The effective mass of an electron at the bottom of the conduction band is equal to 0.18 m_0, with m_0 the free electron mass.

Time-resolved THz photoconductivity measurements were performed on InSe nanosheets drop-casted onto a quartz substrate. The samples were photoexcited with 60 fs laser pulses at 480 nm

(2.6 eV, see Experimental and Methods). Results from the THz photoconductivity measurements data are displayed in Figs. 3 and 4. Photoexcitation can yield free independently moving electrons and holes, as well as neutral excitons that consist of a Coulombically bound electron-hole pair. Motion of free charges with a velocity component in-phase with the oscillating THz field give rise to the real component of the photoconductivity, which can be obtained from reduction of the amplitude of the THz electric field strength.[18-19] Motion of free charges with a velocity component out-of-phase with the THz field, as well as the polarizability of excitons, lead to an imaginary component of the photoconductivity, which can be determined from the phase-retardation of the THz electric field.[18-19]

Fig. 3a shows the quantity $S(t) = \Phi_e(t)\mu_e + \Phi_h(t)\mu_h$, as a function of time, t, after photoexcitation, which is the sum of the product of the quantum yield of electrons, $\Phi_e(t)$ and holes, $\Phi_h(t)$, and the real mobility component of their mobility, (μ_e and μ_h), averaged over a frequency range of 0.3-0.7 THz. At early times, the real THz conductivity exhibits a fast decay with a value $S(t) = 20 \pm 2$ cm^2/Vs after ~4 ps. The ultrafast initial decay is assigned to the relaxation of highly mobile hot charges to the band edge, where the mobility appears to be lower (see Fig. 3a inset).[20-22] Decay on longer times occurs due to recombination and/or trapping of the charge carriers. The decay for the higher photoexcitation density (red, $N_a = 9.7 \times 10^{13}$ photons/cm^2) in Fig 3a is somewhat faster than for the lower density (black, $N_a = 1.5 \times 10^{13}$ photons/cm^2, see Fig. S2 for more photoexcitation densities). This can be understood, since on increasing the charge carrier density higher-order radiative- and Auger-recombination become faster. The signal $S(t)$ was found to be similar for photoexcitation densities lower than 4.7×10^{13} photons/cm^2. Hence, for these lower densities effects of Coulomb interactions on charge mobility and higher-order recombination can be neglected. In addition, an increase of the stabilizing ligand length of InSe

nanosheets from decyl- to octadecylamine did not affect the results for *S(t)*. We conclude that the distance between the stacked nanosheets does not influence the dynamics of charge carriers.

Fig. 3b shows that the decay kinetics of the real and imaginary components of the normalized THz conductivity are the same for low excitation density (1.5×10^{13} photons/cm^2). This means that at low density the contribution of excitons to the imaginary conductivity is negligible. Interestingly, Fig. 3c shows that for higher photoexcitation density (9.7×10^{13} photons/cm^2), the normalized imaginary THz conductivity on times below 200 ps is larger than the real component. This contribution to the imaginary conductivity increases with photoexcitation density, see Fig. S3. The increase of the imaginary conductivity can be understood from the larger fraction of excitons resulting from enhanced recombination of electrons and holes at higher photoexcitation density. The fraction of excitons can be calculated from the 2D Saha equation for the equilibrium between excitons and free charges:[23]

$$\frac{n_{eh}^2}{n^*} = \frac{k_B T}{2\pi\hbar^2}\,\mu\, e^{-E_{2D}/k_B T} \qquad (1)$$

with n_{eh} the 2D density of pairs of free electrons and holes, n^* the exciton density, k_B the Boltzmann's constant, T the temperature, $\hbar$ the reduced Planck constant, μ the reduced effective mass of the electron and hole and E_{2D} the 2D exciton binding energy. The fraction of excitons is given by $f_x = n^*/N$ with $N = n_{eh} + n^*$ the total density of excitons and pairs of free electrons and holes. N can be estimated as $I_0 F_A \frac{d}{\alpha}$ with I_0 the incident photon density per unit area (pump laser fluence), F_A = 60 % the fraction of photons absorbed by the InSe nanosheets (hence $I_0 F_A$ is the photoexcitation density N_a given in Figs. 3, S2, S3 and S4), d ~ 1 nm the thickness of a nanosheet and α = 10^4 cm^{-1} the absorption coefficient of InSe[24]. We assume the 2D exciton binding energy E_{2D} = 0.06 eV, to be four times[25] the bulk value (0.015 eV)[13, 15]. The reduced

effective mass $\mu = 0.18\, m_0$ is obtained from our DFT calculations (see Experimental and Methods). Using equation (1) with these parameter values, yields an exciton fraction $f_x = 0.05$ for the low photoexcitation density of 1.5×10^{13} cm$^{-2.}$, in agreement with the absence of a significant contribution of excitons to the THz conductivity in Fig. 3b. At the highest density (9.7×10^{13} cm^{-2}), we calculate a significant exciton fraction $f_x = 0.22$, which explains the contribution of excitons to the THz conductivity on times below 200 ps in Fig. 3c (see Fig. S4 for an increase of the contribution of excitons to the imaginary THz conductivity with increasing photoexcitation density).

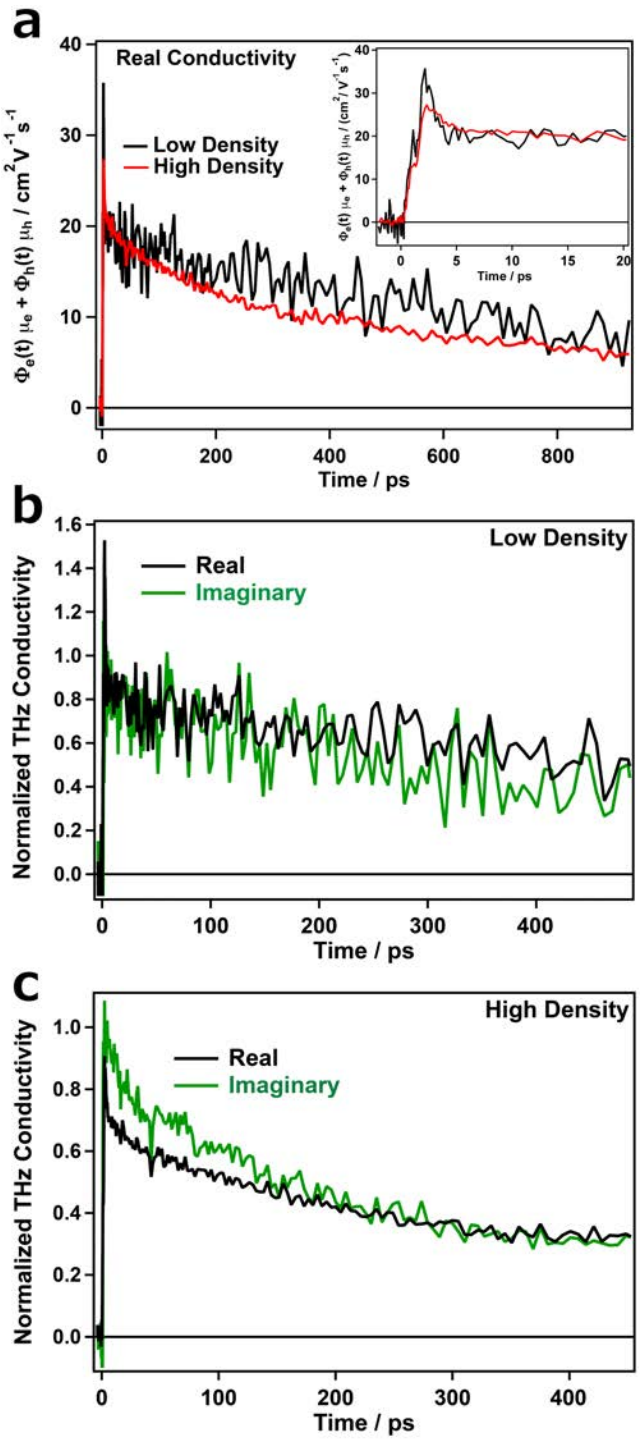

Fig. 3. a) Sum of the product of the quantum yield Φ of electrons and holes and their real mobility, averaged over a frequency range of 0.3 – 0.7 THz for low (black) and high (red) photoexcitation densities of 1.5×10^{13} resp. 9.7×10^{13} cm^{-2}. The ultrafast initial decay on times below 4 ps (see inset) is assigned to relaxation of hot charge carriers to the band edge. After the initial relaxation, the sum of the electron and hole mobility equals 20 ± 2 cm^2/Vs, **b)** Normalized

real and imaginary THz conductivity (low density: 1.5×10^{13} photons/cm^2) plotted on top of each other exhibit the same decay kinetics, which underpins the formation of mainly free charge carriers, **c)** Normalized real and imaginary THz conductivity at a higher photoexcitation density with the decay of the real and imaginary conductivity exhibiting significant differences. Up to 200 ps, the imaginary conductivity shows an additional contribution due to an increased fraction of excitons at higher photoexcitation density.

Fig. 4 shows the sum of the electron and hole mobilities as a function of frequency, as obtained from the THz conductivity at times 8-12 ps after the pump pulse; i.e. when the charges have relaxed to the band edges. The increase of the mobility and the negative imaginary component with frequency is typical for effects of backscattering on charge motion as has been discussed before.[18, 20, 26-29] Such backscattering can result from disorder in the energetic landscape of charges in the InSe nanosheets due to varying conformations of the organic ligands or stacking faults. The real mobility of InSe nanosheets is as high as 20 ± 2 cm^2/Vs at frequencies between 0.3 – 0.7 THz. This value is the first mobility determined for ultrathin colloidal InSe nanosheets stabilized by organic ligands.

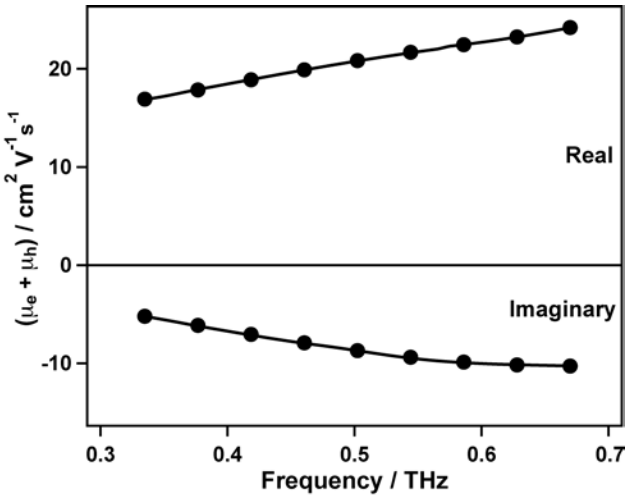

Fig. 4. Frequency dependence of the charge mobility in photoexcited InSe nanosheets, averaged over pump-probe delays of 8 – 12 ps. The increasing real and imaginary mobility at higher THz frequencies is typical for charges moving between transport barriers.

Recent studies on DC mobilities of charges in exfoliated InSe report values as high as 1000 cm^2/Vs.[5, 8] However, the authors describe the mobilities to be highly dependent not only on the thickness of the InSe (1000 cm^2/Vs for a 35 nm thick InSe layer), but also on the dielectric interface/layer used for the production of the FET devices. The thinnest InSe layers studied in FETs were 10 nm thick and deposited on a simple SiO_2 dielectric, yielding a low mobility of 2.2 cm^2/Vs that could be enhanced to 208 cm^2/Vs by modifying the dielectric to PMMA/SiO_2.[8] The authors account the huge differences in the mobilities to interfacial Coulomb impurities that lead to scattering of the charge carriers and reduced mobilities in simple SiO_2-based devices.[8]

The variation of the results on the mobility of InSe underpins the need for a method to determine the "intrinsic" mobility of the compound of interest. Time-resolved terahertz spectroscopy as non-contact AC mobility probe for straightforward wet-chemically processed ultrathin InSe nanosheets yields a mobility as high as 20 ± 2 cm^2/Vs, without effects resulting from a dielectric interface. We estimate a near unity free charge carrier quantum yield in ultrathin InSe under low photoexcitation density, making it a desirable material for ultrathin electronic applications.

EXPERIMENTAL AND METHODS SECTION

The modified synthesis of InSe nanosheets is described in the Supporting Information; the original synthesis can be found in ref. 9.

THz Conductivity Measurements

The frequency dependent mobility of charge carriers in ultrathin InSe nanosheets was determined by time-domain THz spectroscopy. The laser system used has been described for transient absorption and THz conductivity measurements previously[29-31] and data acquisition is briefly

discussed here.[18, 29-32] InSe nanosheets are excited with 60 fs laser pulses and the conductivity due to the generation of free charges and/or excitons is probed by measuring the change of the amplitude and phase of the THz electric field waveform. This yields the conductivity $\Delta\sigma(\omega, t)$ as a function of the frequency, $f = \omega/2\pi$, of the probing THz field at a varying time *t* after the pump pulse. The frequency dependent conductivity due to charges is determined by the field-induced drift velocity in the oscillating THz electric field $E(t) = E_0\cos(\omega, t)$. The complex valued mobility of charges and excitons can be related to three different velocity components in the THz field: 1) The velocity of free charges in-phase with the THz field $v(t) = \mu_R(\omega)E_0\cos(\omega, t)$ with $\mu_R(\omega)$ the real component of the charge mobility, 2) the velocity of free charges out-of-phase with the THz field $v(t) = \mu_I(\omega)E_0\sin(\omega, t)$, with $\mu_I(\omega)$ the imaginary component of the charge mobility, and 3) the relative out-of-phase velocity of an electron and hole that are Coulombically bound $v_{eh}(t) = \mu_I(\omega)E_0\sin(\omega, t)$ with $\mu_I(\omega) = \frac{\alpha\omega}{e}$ and α the polarizability of the exciton.

A home-built set-up includes the detection of the transmitted THz probe by a single-cycle THz pulse, generated in a $LiNbO_3$ crystal and detected in a ZnTe crystal. A chirped optical pulse used for spectral encoding, allows a single shot detection of the THz waveform. From the measurements we obtain the differential transmission of the THz waveform $\Delta E(t_p, t) = E_{excited}(t_p, t) - E_0(t_p)$ with $E_{excited}(t_p, t)$ the transmitted THz electric field after photoexcitation of the sample and $E_0(t_p)$ the transmitted THz electric field in absence of photoexcitation, t_p is the time between generating and detecting the THz field and t the time delay between the photoexcitation pump pulse and the THz probe pulse. $\Delta E(t_p, t)$ is normalized to E_{max}, the maximum amplitude of the transmitted THz field in absence of pumping. The

complex, frequency-dependent conductivity with respect to the THz time delay t_p is then extracted by applying the Fourier transform $F(\omega) = \int_{-\infty}^{\infty} f(t_p) e^{i\omega t_p} dt_p$ and yields:

$$\frac{\Delta E(\omega,t)}{E_0(\omega)} = -\frac{\Delta\sigma(\omega,t)L}{2c\varepsilon_0\sqrt{\varepsilon(\omega)}} \qquad (2)$$

where c is the speed of light, L is the thickness of the sample, ε_0 is the vacuum permittivity, and $\varepsilon(\omega)$ is the dielectric function of the sample. $\sqrt{\varepsilon(\omega)} = n_{eff} = 3$ is the effective refractive index of InSe at THz frequencies.[33] Using the real conductivity due to free charges only $\Delta\sigma = e(n_e\mu_e + n_h\mu_h)$ with e the elementary charge, μ_e (μ_h) the mobility of electrons (holes) and $n_e(n_h)$ the average density of electrons (holes). For an absorbed photoexcitation density per unit area $N_a = I_0 F_A$ (I_0 is the pump laser fluence (incident photon density per unit area), F_A is the fraction of photons absorbed), $n_{e,h} = \Phi_{e,h}(t) N_a / L$, we can determine the sum of the product of the photogeneration charge carrier quantum yield and the electron and hole mobility as:

$$\phi_e(t)\mu_e + \phi_h(t)\mu_h = -\frac{\Delta E(\omega,t)}{E_0(\omega)} \frac{2c\varepsilon_0 n_{eff}}{eN_a} \qquad (3)$$

Note that equation (3) does not require the actual sample thickness L, but only the photoexcitation density N_a per unit area.

DFT Calculations

The band structure of a single InSe monolayer was calculated at the density functional level of theory (DFT). These calculations were performed with the BAND program included in the Amsterdam Density Functional (ADF) package.[34] A single unit cell containing 2 In atoms and 2 Se atoms was considered with periodic boundary conditions only in the plane of the monolayer as BAND allows true two-dimensional calculations. The geometric structure of the monolayer was first optimized using a small DZP basis set and the Local Density Approximation (LDA) to compute the exchange and correlation functional. The relaxed geometry at the DZP/LDA level

was then used to compute the band structure at higher level of theories. We have used a larger basis set here, namely TZ2P and the PBE functional to evaluate the electronic structure of the material. Spin-orbit coupling is explicitly included in the calculations. The charge effective masses were calculated from the curvature of the band edges. The curvature was calculated by diagonalization of the Hessian matrix. This lead to effective masses of $m_1 = -8.85\, m_0$ and $m_2 = -54.36\, m_0$ for the holes and $m_1 = m_2 = 0.18\, m_0$ for the electrons. Note the large anisotropy of the hole effective mass due to the shift of the valence band maximum away from the Γ point.

TEM Characterization

TEM imaging was conducted with a JEOL-JEM 1400 operating at 120 kV.

Optical Characterization

Optical absorption spectra of thin films and solutions in toluene were measured with a PerkinElmer Lambda 1050 spectrometer equipped with an integrating sphere.

ASSOCIATED CONTENT

Supporting Information. InSe nanosheet synthesis, additional absorption and photoluminescence measurements, real and imaginary THz conductivity for a range of photoexcitation densities. This material is available free of charge via the Internet at http://pubs.acs.org.

AUTHOR INFORMATION

Corresponding Author

Jannika Lauth*, j.d.lauth@tudelft.nl,

Laurens D. A. Siebbeles*, l.d.a.siebbeles@tudelft.nl

REFERENCES

(1) Bhimanapati, G. R.; Lin, Z.; Meunier, V.; Jung, Y.; Cha, J.; Das, S.; Xiao, D.; Son, Y.; Strano, M. S.; Cooper, V. R., *et al*. Recent Advances in Two-Dimensional Materials beyond Graphene. *ACS Nano* **2015,** *9*, 11509-11539.

(2) Zhang, H. Ultrathin Two-Dimensional Nanomaterials. *ACS Nano* **2015,** *9*, 9451-9469.

(3) Butler, S. Z.; Hollen, S. M.; Cao, L.; Cui, Y.; Gupta, J. A.; Gutiérrez, H. R.; Heinz, T. F.; Hong, S. S.; Huang, J.; Ismach, A. F., *et al*. Progress, Challenges, and Opportunities in Two-Dimensional Materials Beyond Graphene. *ACS Nano* **2013,** *7*, 2898-2926.

(4) Wang, Q. H.; Kalantar-Zadeh, K.; Kis, A.; Coleman, J. N.; Strano, M. S. Electronics and Optoelectronics of Two-Dimensional Transition Metal Dichalcogenides. *Nat. Nanotechnol*. **2012,** *7*, 699-712.

(5) Sucharitakul, S.; Goble, N. J.; Kumar, U. R.; Sankar, R.; Bogorad, Z. A.; Chou, F.-C.; Chen, Y.-T.; Gao, X. P. A. Intrinsic Electron Mobility Exceeding 10^3 cm^2/(Vs) in Multilayer InSe FETs. *Nano Lett*. **2015,** *15*, 3815–3819.

(6) Aerts, M.; Bielewicz, T.; Klinke, C.; Grozema, F. C.; Houtepen, A. J.; Schins, J. M.; Siebbeles, L. D. A. Highly Efficient Carrier Multiplication in PbS Nanosheets. *Nat. Commun*. **2014,** *5*, 3789.

(7) Lei, S.; Wen, F.; Ge, L.; Najmaei, S.; George, A.; Gong, Y.; Gao, W.; Jin, Z.; Li, B.; Lou, J., *et al*. An Atomically Layered InSe Avalanche Photodetector. *Nano Lett*. **2015,** *15*, 3048-3055.

(8) Feng, W.; Zheng, W.; Cao, W.; Hu, P. Back Gated Multilayer InSe Transistors with Enhanced Carrier Mobilities via the Suppression of Carrier Scattering from a Dielectric Interface. *Adv. Mater*. **2014,** *26*, 6587-6593.

(9) Lauth, J.; Gorris, F. E. S.; Samadi Khoshkhoo, M.; Chassé, T.; Friedrich, W.; Lebedeva, V.; Meyer, A.; Klinke, C.; Kornowski, A.; Scheele, M., *et al*. Solution-Processed Two-Dimensional Ultrathin InSe Nanosheets. *Chem. Mater*. **2016,** *28*, 1728-1736.

(10) Hergert, F.; Jost, S.; Hock, R.; Purwins, M. A Crystallographic Description of Experimentally Identified Formation Reactions of Cu(In,Ga)Se2. *J. Solid State Chem*. **2006,** *179*, 2394-2415.

(11) Imai, K.; Suzuki, K.; Haga, T.; Hasegawa, Y.; Abe, Y. Phase Diagram of Indium-Selenide System and Crystal Growth of Indium Monoselenide. *J. Cryst. Growth* **1981,** *54*, 501-506.

(12) Novoselov, K. S.; Geim, A. K.; Morozov, S. V.; Jiang, D.; Zhang, Y.; Dubonos, S. V.; Grigorieva, I. V.; Firsov, A. A. Electric Field Effect in Atomically Thin Carbon Films. *Science* **2004,** *306*, 666-669.

(13) Madelung, O. *Semiconductors: Data Handbook*. 3 ed.; Springer: London, 2003.

(14) Brotons-Gisbert, M.; Andres-Penares, D.; Suh, J.; Hidalgo, F.; Abargues, R.; Rodríguez-Cantó, P. J.; Segura, A.; Cros, A.; Tobias, G.; Canadell, E, *et al*. Nanotexturing To Enhance Photoluminescent Response of Atomically Thin Indium Selenide with Highly Tunable Band Gap. *Nano Lett*. **2016,** *16*, 3221-3229.

(15) Mudd, G. W.; Svatek, S. A.; Ren, T.; Patanè, A.; Makarovsky, O.; Eaves, L.; Beton, P. H.; Kovalyuk, Z. D.; Lashkarev, G. V.; Kudrynskyi, Z. R., *et al*. Tuning the Bandgap of Exfoliated InSe Nanosheets by Quantum Confinement. *Adv. Mater*. **2013,** *25*, 5714-5718.

(16) Debbichi, L.; Eriksson, O.; Lebègue, S. Two-Dimensional Indium Selenides Compounds: An Ab Initio Study. *J. Phys. Chem. Lett*. **2015,** *6*, 3098-3103.

(17) Zólyomi, V.; Drummond, N. D.; Fal'ko, V. I. Electrons and Phonons in Single Layers of Hexagonal Indium Chalcogenides from *Ab Initio* Calculations. *Phys. Rev. B* **2014,** *89*, 205416.
(18) Ulbricht, R.; Hendry, E.; Shan, J.; Heinz, T. F.; Bonn, M. Carrier Dynamics in Semiconductors Studied with Time-Resolved Terahertz Spectroscopy. *Rev. Mod. Phys.* **2011,** *83*, 543-586.
(19) Lloyd-Hughes, J.; Jeon, T.-I. A Review of the Terahertz Conductivity of Bulk and Nano-Materials. *J. Infrared Millim. Terahertz Waves* **2012,** *33*, 871-925.
(20) Alberding, B. G.; Biacchi, A. J.; Hight Walker, A. R.; Heilweil, E. J. Charge Carrier Dynamics and Mobility Determined by Time-Resolved Terahertz Spectroscopy on Films of Nano-to-Micrometer-Sized Colloidal Tin(II) Monosulfide. *J. Phys. Chem. C* **2016,** *120*, 15395-15406.
(21) Gao, Y.; Talgorn, E.; Aerts, M.; Trinh, M. T.; Schins, J. M.; Houtepen, A. J.; Siebbeles, L. D. A. Enhanced Hot-Carrier Cooling and Ultrafast Spectral Diffusion in Strongly Coupled PbSe Quantum-Dot Solids. *Nano Lett.* **2011,** *11*, 5471-5476.
(22) Strait, J. H.; Wang, H.; Shivaraman, S.; Shields, V.; Spencer, M.; Rana, F. Very Slow Cooling Dynamics of Photoexcited Carriers in Graphene Observed by Optical-Pump Terahertz-Probe Spectroscopy. *Nano Lett.* **2011,** *11*, 4902-4906.
(23) Kaindl, R. A.; Carnahan, M. A.; Hägele, D.; Chemla, D. S. Ultrafast THz Spectroscopy of Excitons in Multi-Component Carrier Gases. In *Advances in Solid State Physics*, Haug, R., Ed. Springer Berlin Heidelberg: 2008; Vol. 47, pp 191-202.
(24) Chaudhuri, S.; Biswas, S. K.; Choudhury, A. Dependence of Optical Absorption of Amorphous InSe Films on Temperature of Heat Treatment. *Solid State Commun.* **1985,** *53*, 273-276.
(25) Orton, J. W. *The Story of Semiconductors*. Oxford University Press Inc.: New York, 2004.
(26) Turner, G. M.; Beard, M. C.; Schmuttenmaer, C. A. Carrier Localization and Cooling in Dye-Sensitized Nanocrystalline Titanium Dioxide. *J. Phys. Chem. B* **2002,** *106*, 11716-11719.
(27) Hilt, O.; Siebbeles, L. D. A. Time and Frequency Dependent Charge Carrier Mobility of One-Dimensional Chains with Energetic Disorder. *Chem. Phys. Lett.* **1997,** *269*, 257-262.
(28) Grozema, F. C.; Siebbeles, L. D. A. Mechanism of Charge Transport in Self-Organizing Organic Materials. *Int. Rev. Phys. Chem.* **2008,** *27*, 87-138.
(29) Evers, W. H.; Schins, J. M.; Aerts, M.; Kulkarni, A.; Capiod, P.; Berthe, M.; Grandidier, B.; Delerue, C.; van der Zant, H. S. J.; van Overbeek, C., *et al*. High Charge Mobility in Two-Dimensional Percolative Networks of PbSe Quantum Dots Connected by Atomic Bonds. *Nat. Commun.* **2015,** *6*, 8195.
(30) Kunneman, L. T.; Schins, J. M.; Pedetti, S.; Heuclin, H.; Grozema, F. C.; Houtepen, A. J.; Dubertret, B.; Siebbeles, L. D. A. Nature and Decay Pathways of Photoexcited States in CdSe and CdSe/CdS Nanoplatelets. *Nano Lett.* **2014,** *14*, 7039-7045.
(31) Kunneman, L. T.; Zanella, M.; Manna, L.; Siebbeles, L. D. A.; Schins, J. M. Mobility and Spatial Distribution of Photoexcited Electrons in CdSe/CdS Nanorods. *J. Phys. Chem. C* **2013,** *117*, 3146-3151.
(32) Murphy, J. E.; Beard, M. C.; Nozik, A. J. Time-Resolved Photoconductivity of PbSe Nanocrystal Arrays. *J. Phys. Chem. B* **2006,** *110*, 25455-25461.

(33) Sardarly, R. M.; Garet, F.; Bernier, M.; Coutaz, J.-L. Characterization of Selenide, Sulfide and Telluride Materials by Terahertz Time-Domain Spectroscopy. In *Terahertz and Mid Infrared Radiation: Detection of Explosives and CBRN (Using Terahertz) in NATO Science for Peace and Security Series B: Physics and Biophysics* Pereira, M. F.; Shulika, O., Eds. Springer Netherlands: 2014; pp 129-133.
(34) Philipsen, P. H. T.; te Velde, G.; Baerends, E. J.; Berger, J. A.; de Boeij, P. L.; Franchini, M.; Groeneveld, J. A., BAND2013, *ADF: Powerful DFT Software*, SCM, Theoretical Chemistry, Vrije Universiteit Amsterdam, The Netherlands, http://www.scm.com, last accessed 07/03/2016.